

Supplementary Materials for **Wavelength-tunable and shape-reconfigurable photonic capsule resonators containing cholesteric liquid crystals**

Sang Seok Lee, Jong Bin Kim, Yun Ho Kim, Shin-Hyun Kim

Published 22 June 2018, *Sci. Adv.* **4**, eaat8276 (2018)

DOI: 10.1126/sciadv.aat8276

The PDF file includes:

- section S1. Microfluidic production of triple-emulsion drops
- section S2. Photonic cross-communication in CLC capsule array
- section S3. Optical setup for measurement of emission from CLC capsules
- section S4. Temperature dependence of photonic stop-band of CLC solution
- section S5. Competition between SWE and LWE
- section S6. Temperature-dependent threshold energy
- section S7. Input energy on the flattened area of deformed capsule
- section S8. Enhancement of lasing intensity and reduction of FWHM during incubation
- fig. S1. Preparation of triple-emulsion drops using a capillary microfluidic device.
- fig. S2. Photonic cross-communication.
- fig. S3. Optical setup for emission measurement from capsules.
- fig. S4. Tuning of photonic stop band with temperature.
- fig. S5. Competition between SWE and LWE for lasing.
- fig. S6. Temperature-dependent threshold energy.
- fig. S7. Input energy on the flattened area of deformed capsule.
- fig. S8. Enhancement of laser quality over incubation.

Other Supplementary Material for this manuscript includes the following:
(available at advances.sciencemag.org/cgi/content/full/4/6/eaat8276/DC1)

- movie S1 (.mp4 format). Spontaneous healing of oily streak in deformed capsule.

section S1. Microfluidic production of triple-emulsion drops

To prepare O/W/O/W triple-emulsion drops as a template for capsules, a capillary microfluidic device is used. The device consists of two tapered glass cylindrical capillaries which are assembled in a square capillary (fig. S1). One of the cylindrical capillary is chemically modified to have hydrophilic inner wall and hydrophobic outer wall. The other capillary is treated to have hydrophilic inner and outer walls. The device produces O/W/O/W triple-emulsion drops with ultra-thin inner water layer with a thickness of approximately 2 μm ; the inner shell is not discernible in optical microscope (OM) image.

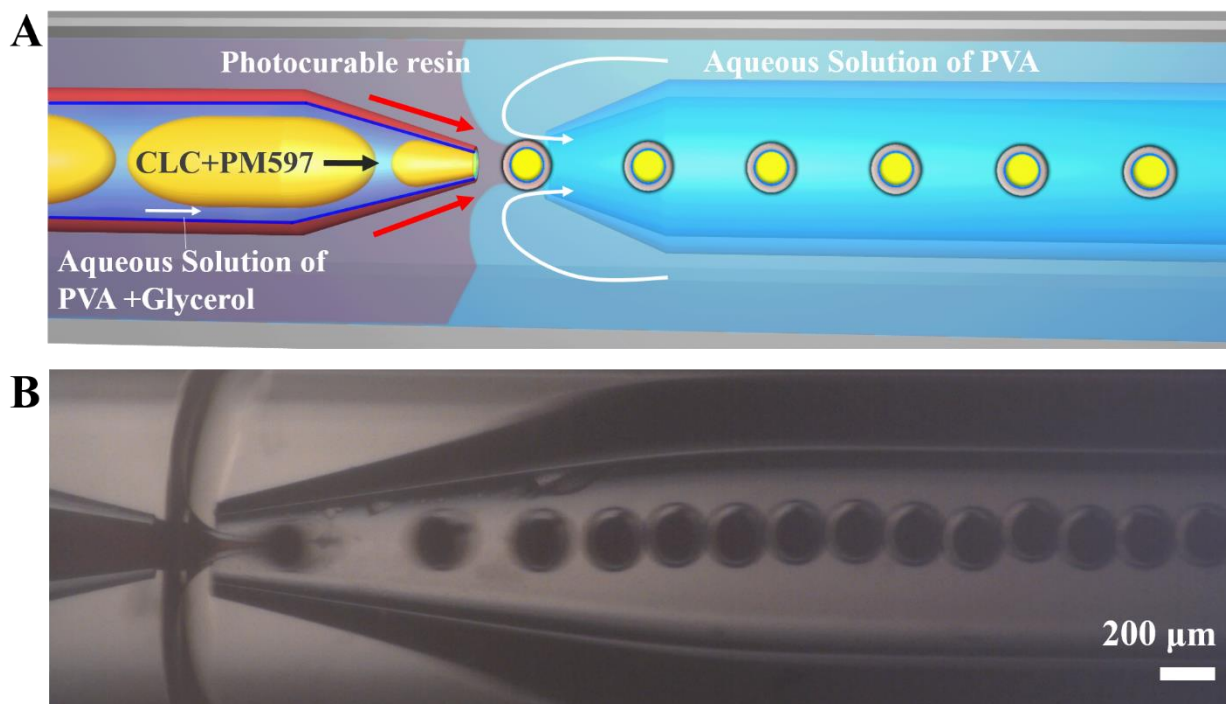


fig. S1. Preparation of triple-emulsion drops using a capillary microfluidic device. (A) Schematic for device construction. **(B)** Still-shot optical microscope (OM) image showing the junction of the microfluidic device where triple-emulsion drops are produced.

section S2. Photonic cross-communication in CLC capsule array

When CLC drops have a planar alignment along the spherical interface, the helical axes are radially organized. Therefore, the CLC drops are isotropic and show rotation-independent reflection at stop band. When 2D array of CLC drops is irradiated by collimated light, each drop shows a strong reflection on the central area as the light is normally reflected; the wavelength of reflection is $n_{av}P$. At the same time, the drops show additional reflection pattern through photonic cross-communication (26, 27). The incident light is first reflected by a drop at the polar angle of 45° , which is reflected again by a neighboring drop at the same angle, as denoted with a path “2” in fig. S2A. Therefore, the number of dots is the same to that of neighbors that participate the dual reflection path. The wavelength of reflection is $n_{av}P\cos 45^\circ$. This color pattern caused by path “2” always appears regardless of the surrounding condition as long as CLC drops have a high quality of radially-oriented helical structures. When the 2D array is immersed in a liquid, there is another light path that can produce additional color pattern. The incident light is first reflected by a drop above the polar angle of 45° , which is second reflected at air-liquid interface and finally reflected by a neighboring drop at the same angle, as denoted with a path “3”. This color pattern appears only when the level of the liquid medium is in a certain range and angle of reflection varies with the level. The CLC capsules have high quality of radially-oriented helical structures because aqueous inner shell causes the planar alignment along the interface. Therefore, the capsules show both color patterns through the paths “2” and “3” when the level of surrounding water is slightly higher than the diameter of the capsules (fig. S2B). When the level is much higher, only the pattern by the path “2” is shown (fig. S2C).

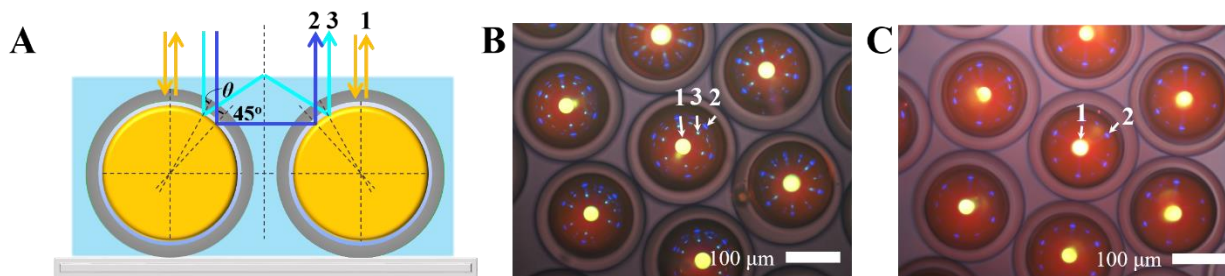


fig. S2. Photonic cross-communication. (A) Schematic diagram showing the light paths of normal reflection (path 1) and photonic cross-communications between two neighbors (paths “2” and “3”). (B) OM image of CLC capsules immersed in a low level of water. Each capsule shows a central yellow dot through normal reflection, series of blue dots through the photonic cross-communication with the path “2”, and series of green dots through the cross-communication with the path “3”. (C) OM image of CLC capsules immersed in a high level of water. The capsules show a central dot and series of blue dots in the absence of series of green dots as the path “3” is not available.

section S3. Optical setup for measurement of emission from CLC capsules

A Nd:YAG laser in 2nd harmonics is used as a pumping laser. The laser beam passes through the first polarizing beam-splitter (PBS), a half-wave plate, the second PBS, a quarter-wave plate, and lens before hitting the capsules (fig. S3). At the first PBS, P-polarized beam is transmitted, which is then rotated to an angle of $2\theta = 45^\circ$ to the fast axis by the half-wave plate. At the second PBS, the rotated beam with an angle of 45° is separated into S- and P-polarized beams with a ratio of 50:50. The S-polarized beam hits an energy meter and P-polarized beam is changed a left-handed circularly-polarized light by the quarter-wave plate. The circularly-polarized light is focused on the sample stage with a spot diameter of $800 \mu\text{m}$ by the lens. The left-handed circularly-polarized light hits the capsules with an incident angle of 45° and the emission from the capsules is measured with the fiber-coupled spectrometer in surface normal direction to the stage. During the optical pumping, the capsules are observed with a CCD camera from the opposite side to the spectrometer. The intensity of the pumping laser is adjusted by Q-switch delay time.

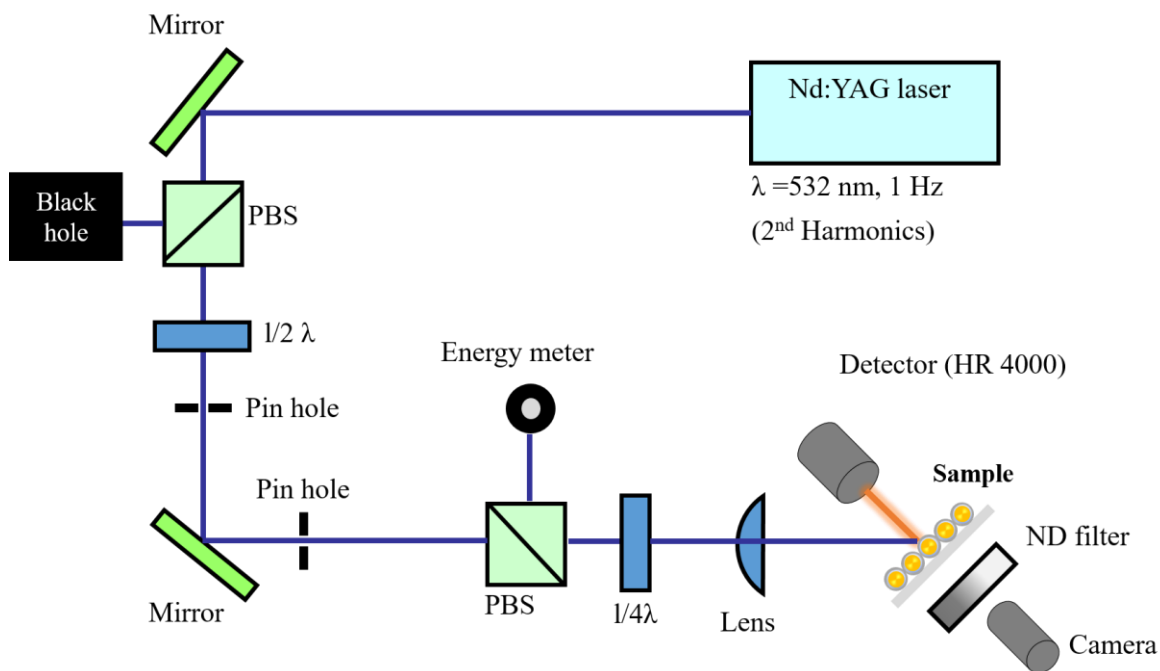


fig. S3. Optical setup for emission measurement from capsules.

section S4. Temperature dependence of photonic stop-band of CLC solution

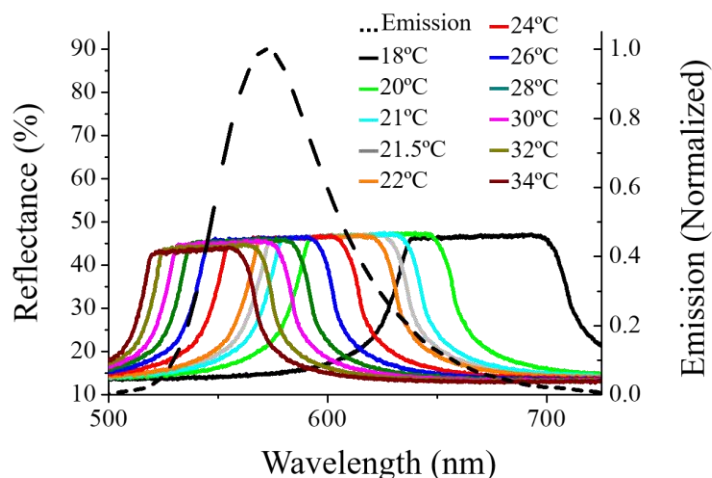


fig. S4. Tuning of photonic stop band with temperature. The reflectance spectra of CLC solution infiltrated in a planar cell with a thickness of 50 μm taken at various temperatures as denoted (left y-axis). The CLC solution is a mixture of 0.68 w/w% R5011, 19.8 w/w% R811, and 79.52 w/w% E7 liquid crystal. The spontaneous emission of PM 597 dye dissolved in the mixture at 60°C (right axis). The LC molecules form isotropic phase at the temperature.

section S5. Competition between SWE and LWE

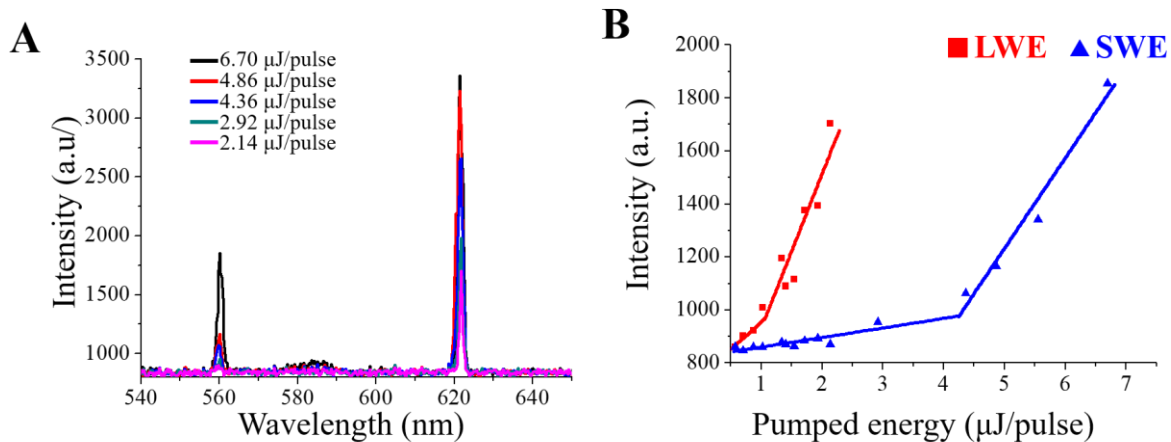


fig. S5. Competition between SWE and LWE for lasing. (A) Series of the emission spectra from CLC capsule at 22°C with various pumped energies. (B) The emission intensities in the short-wavelength edge (SWE, blue triangles) and long-wavelength edge (LWE, red squares) as a function of the pumped energy. The threshold energy in SWE is 4.25 $\mu\text{J}/\text{pulse}$ and that in LWE is 1.05 $\mu\text{J}/\text{pulse}$, indicating that the lasing in LWE is preferred.

section S6. Temperature-dependent threshold energy

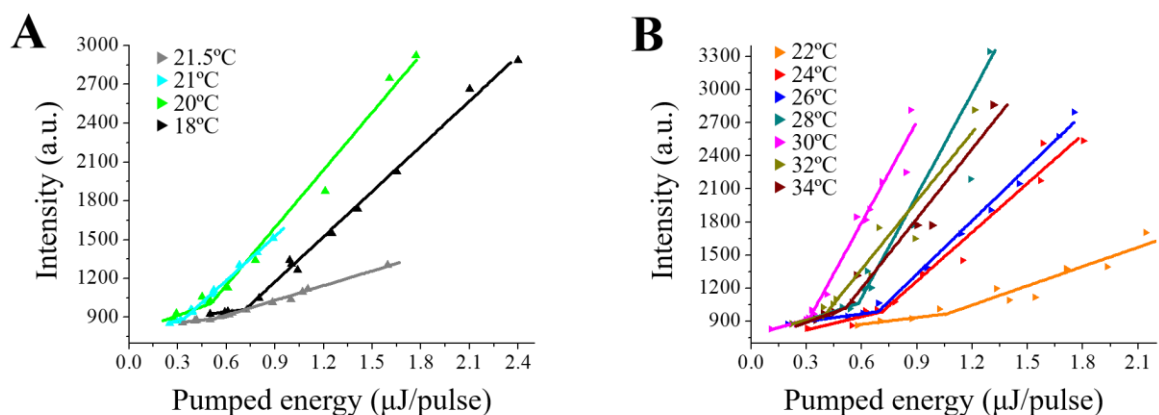


fig. S6. Temperature-dependent threshold energy. (A) The emission intensities in SWE from CLC capsule as a function of the pumped energy in the temperature range of 18 – 21.5°C, where SWE blue-shifts as the temperature increases. (B) The same in LWE in the temperature range of 22 – 34°C. Temperature-dependent (or wavelength-dependent) threshold energies are extracted from the plots for SWE and LWE in the full temperature range of 18 – 34°C.

section S7. Input energy on the flattened area of deformed capsule

The intensity profile of pumping source follows the Gaussian distribution

$$I(r) = I_0 \exp\left(-\frac{2r^2}{w_0^2}\right)$$

where $I(r)$ is intensity at a distance (r) from the center, I_0 is the maximum intensity at $r = 0$, and w_0 is the Gaussian radius at which the amplitude is $1/e$ of the maximum intensity; $w_0 = 358 \mu\text{m}$. The input energy on the flattened area of deformed capsule is estimated by integrating the intensity distribution from $r = 0$ to the radius of the flattened area.

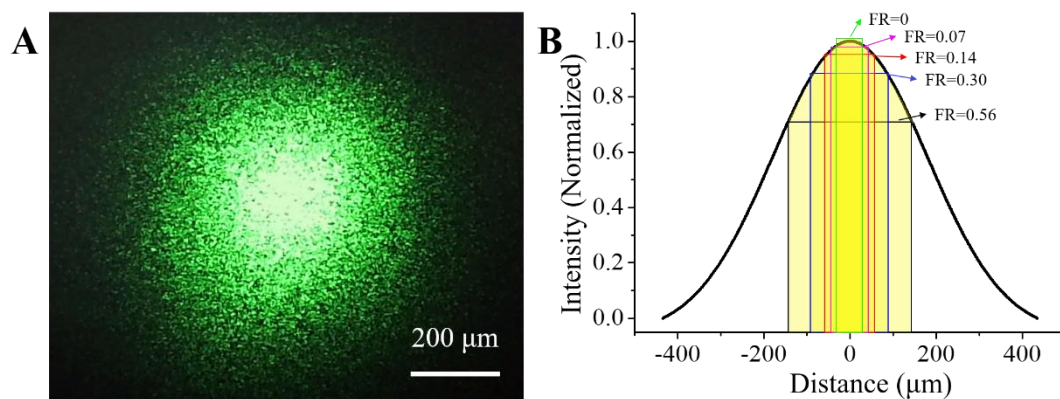


fig. S7. Input energy on the flattened area of deformed capsule. (A) Photograph of the optical pumping source of which intensity follows Gaussian distribution. (B) Gaussian distribution with a Gaussian radius of $w_0 = 358 \mu\text{m}$. For deformed capsules with various flattening ratios (FRs), the diameters of the flattened area are denoted in the plot.

section S8. Enhancement of lasing intensity and reduction of FWHM during incubation

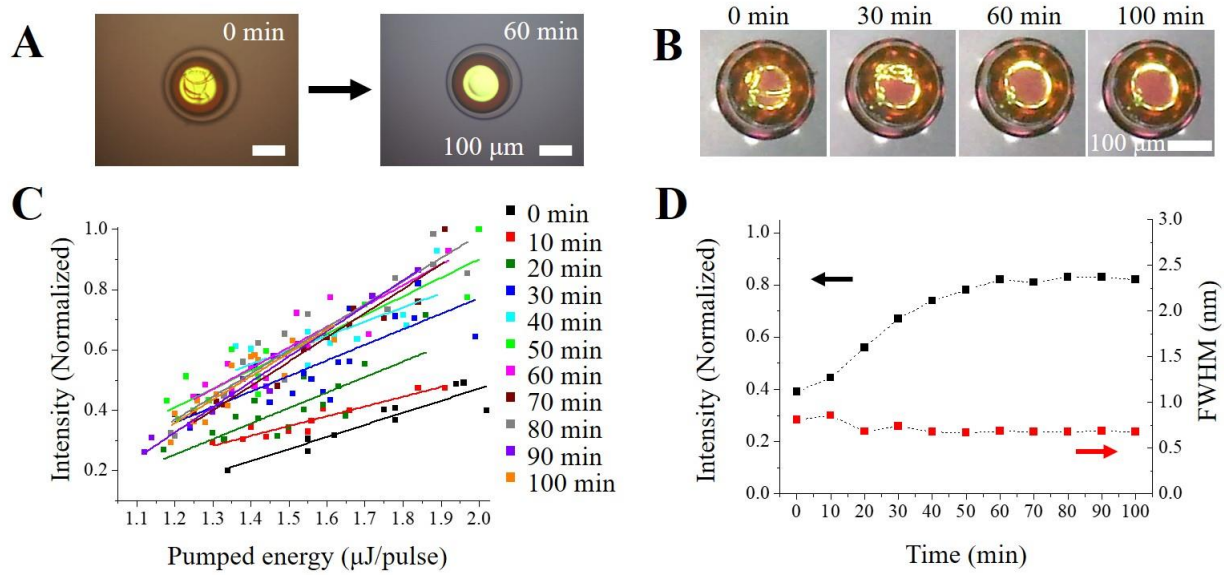


fig. S8. Enhancement of laser quality over incubation. (A) OM images showing spontaneous healing of oily streak over incubation for the deformed capsule with $FR = 0.36$. (B) Images showing the expansion of lasing area upon the healing of oily streak. (C) Lasing intensities from the deformed CLC capsule as a function of pumped energy in LWE over incubation time. (D) The intensity (left y-axis, black squares) and full width at half maximum (FWHM, right y-axis, red squares) of the laser emission with an pumped energy of $1.8 \mu\text{J}/\text{pulse}$ as a function of incubation time. The intensity is saturated in 60 minutes and FWHM remains almost unchanged after 40 minutes.